Data-driven core-collapse supernova multilateration with first neutrino events

Farrukh Azfar,[1] Jeff Tseng,[1,*] Marta Colomer Molla,[2] Kate Scholberg,[3] Alec Habig,[4] Segev BenZvi,[5] Melih Kara,[6] James Kneller,[7] Jost Migenda,[8] Dan Milisavljevic,[9] and Evan O'Connor[10]

[1]*Department of Physics, Oxford University, Oxford OX1 3RH United Kingdom*
[2]*Université Libre de Bruxelles, Bruxelles 1050, Belgium*
[3]*Department of Physics, Duke University, Durham, North Carolina 27708, USA*
[4]*Department of Physics and Astronomy, University of Minnesota Duluth, Duluth, Minnesota 55812, USA*
[5]*Department of Physics and Astronomy, University of Rochester, Rochester, New York 14627, USA*
[6]*Institute for Astroparticle Physics, Karlsruhe Institute of Technology, Karlsruhe 76021, Germany*
[7]*Department of Physics, North Carolina State University, Raleigh, North Carolina 27695, USA*
[8]*e-Research, King's College London, London, United Kingdom*
[9]*Department of Physics and Astronomy, Purdue University, West Lafayette, Indiana 47907, USA*
[10]*The Oskar Klein Centre, Department of Astronomy, Stockholm University, AlbaNova, Stockholm SE-10691, Sweden*

(Received 21 October 2024; accepted 9 February 2026; published 3 March 2026)

A Galactic core-collapse supernova (CCSN) is likely to be observed in neutrino detectors around the world minutes to hours before the electromagnetic radiation arrives. The SuperNova Early Warning System (SNEWS2.0) network of neutrino and dark matter detectors aims to use the relative arrival times of the neutrinos at the different experiments to point back to the supernova so as to facilitate follow-up observation. One of the simplest methods to estimate the CCSN direction is to use the first neutrino events detected through the inverse β decay (IBD) process, $\bar{\nu}_e p \to e^+ n$. We will consider neutrino detectors sensitive to IBD interactions with low backgrounds. The difference in signal arrival times between a large and a small detector will be biased, however, with the first event at the smaller detector, on average, arriving later than that at the larger detector. This bias can be mitigated by using these first events in a data-driven approach without recourse to simulations or models. The resulting method requires, at minimum, only the times of the first events at most detectors, along with a longer time series of events from one larger detector to act as a reference lightcurve. In this article, we demonstrate this method and its uncertainty estimate using pairs of detectors of different sizes and with different supernova distances. Finally, we use this method to calculate probability skymaps using four detectors currently in operation, Super-Kamiokande, Jiangmen Underground Neutrino Observatory (JUNO), Large Volume Detector (LVD), and SNO+, and show that the calculated probabilities yield appropriate confidence intervals for all supernova directions. The area of the 68% confidence interval varies by distance and direction, but is expected to be a few thousand square degrees. The resulting skymaps should be useful for the multimessenger community as a rapid, initial pointing to follow up on the SNEWS2.0 Galactic CCSN neutrino alert.

DOI: 10.1103/t1qp-1q9z

I. INTRODUCTION

The collapse of a massive star in the Milky Way is a unique opportunity rich with physics on topics spanning astrophysics, cosmology, nuclear physics, and fundamental particle physics [1]. At the same time, it is an exceedingly rare phenomenon, with rates estimated to be around 1.63 ± 0.46 per century [8]. In order to take maximal advantage of the next Galactic core-collapse supernova (CCSN), the upgrade of the SuperNova Early Warning System (SNEWS2.0) [9] aims to utilize the burst of neutrinos, which precedes electromagnetic radiation by minutes to hours, to alert the world's observers. The SNEWS2.0 network also aims to use the relative arrival times of the neutrino bursts at each detector to point back to the supernova and guide follow-up observations.

The idea of multilateration (or, informally, "triangulation") using the neutrino arrival times has been explored by multiple authors [10–14]. One of the simplest methods is

*Contact author: jeff.tseng@physics.ox.ac.uk

to use the first observed events to determine the time differences between detector observations. For this method to be effective, the background should be negligible, which is a reasonable assumption for many underground detectors on the approximately ten-second timescale of a supernova burst. In addition to its simplicity, the method has the added advantages of being fast as well as relatively independent of supernova models, and thus works in almost all circumstances. It is expected, of course, that pointing accuracy will ultimately be dominated by neutrino-electron elastic scattering events in large detectors such as Super-Kamiokande [15] and the Deep Underground Neutrino Experiment (DUNE) [16], which expect pointing precisions between 3 and 7 degrees for a distance of 10 kpc, depending on supernova model, but simple multilateration through a combination of detectors can provide added quickness and robustness to the search for multimessenger counterparts.

In this article, we describe a refined first-event method which reduces the inherent bias due to comparing detectors with different event yields, along with a practical data-driven method for estimating directional uncertainty, which is critical for assigning confidence levels to different directions (Sec. II). Section III describes the very simple simulation setup used to evaluate the method's performance, and Sec. IV presents the results of that evaluation. We combine multiple detectors in Sec. V to make skymaps with confidence intervals, and discuss the results in Sec. VI.

II. METHOD

Multilateration involves calculating the most likely direction to the supernova using the differences between arrival times of the neutrino bursts at different detectors. In principle, if the direction to the supernova is given by the unit vector $\hat{\mathbf{n}}$, we can predict the arrival time differences (the "true lags") between two detector positions $\mathbf{r}_A$ and $\mathbf{r}_B$ using the formula

$$\tau_{AB}(\hat{\mathbf{n}}) = -\frac{(\mathbf{r}_A - \mathbf{r}_B)\cdot\hat{\mathbf{n}}}{c}, \tag{1}$$

where we have assumed that the neutrinos travel at the speed of light c. If we measure corresponding time differences Δt_{AB}, we can find the most likely direction by varying $\hat{\mathbf{n}}$ and minimizing the quantity

$$\chi^2(\hat{\mathbf{n}}) = \sum_{AB}\sum_{CD}(\Delta t_{AB} - \tau_{AB}(\hat{\mathbf{n}}))V^{-1}_{AB,CD}(\Delta t_{CD} - \tau_{CD}(\hat{\mathbf{n}})), \tag{2}$$

where the sums are over detector pairs AB and CD, and $V_{AB,CD}$ is the covariance matrix of the time differences. (We will use $\tau_{AB}(\hat{\mathbf{n}})$ to denote the true lag given an arbitrary direction $\hat{\mathbf{n}}$, while τ_{AB} with no explicit dependence will refer to the true lag given the true supernova direction.) It should be obvious that it is important to reduce any biases in determining the time differences Δt_{AB}, as they may guarantee that follow-up observers will be watching the wrong patch of sky for the explosion.

Equally important for multilateration is the estimation of the covariance matrix V, as it determines the size and shape of the confidence intervals, and therefore the size and priority of search areas. Previous methods [12–14] have generally relied on evaluating such uncertainties by running Monte Carlo trials with either model- or data-derived inputs. Such methods are potentially time consuming, and in the case of toy models, may introduce further systematic uncertainties. The other main aim of this paper is to estimate these uncertainties using direct calculations from the data itself.

For this paper, we will focus on four geographically dispersed detectors which are currently in operation and are primarily sensitive to the inverse β decay (IBD) process, $\bar{\nu}_e p \to e^+ n$: Super-Kamiokande (Japan) [17], Jiangmen Underground Neutrino Observatory (JUNO, China) [18], Large Volume Detector (LVD, Italy) [19], and SNO+ (Canada) [20]. The IBD channel possesses advantages of sensitivity to a single antineutrino flavor, a large interaction cross section, and accessibility in a number of operating water Cherenkov and liquid scintillator detectors. Moreover, in detectors which can tag the subsequent neutron capture on protons or, in the case of Super-Kamiokande, on gadolinium nuclei, non-IBD events can be reduced significantly; for this study we assume the background is negligible. We assume further that the neutrino event rates as a function of time observed in every detector differ in their overall normalization but are otherwise nearly identical in shape, i.e., the neutrino events are well above trigger thresholds, and Earth-matter effects are negligible. This assumption is not strictly true for this set of detectors, since Super-Kamiokande applies a 7 MeV energy threshold on the prompt positron; while this threshold is well below the mean energy of 20 MeV expected for observed supernova $\bar{\nu}_e$'s, it introduces a small and mostly negligible delay to its time distribution, which is not taken into account in this method. Finally, we neglect the very small, relatively low energy flux of $\bar{\nu}_e$, indicative of late-stage nuclear burning, which is expected to precede core collapse [21–24].

A. First-event bias

As noted above, one of the simplest methods to calculate the Δt_{AB} is to take the time difference between the first events observed at each detector. This method, however, incurs a significant bias due to the fact that a larger detector will in general see its first event earlier, relative to the beginning of the burst, than a smaller detector. In this section, we derive a method for mitigating this bias.

First, we derive a numerical estimate of the expectation value of the first-event time in one detector. Let t_j be the time of the jth observed event at a single detector, with $j = 1, 2, \ldots N$. The probability density function (PDF) for observing the first event at time t_1 is the product of two probabilities: first, of observing zero events in the time

interval $(-\infty, t_1)$ followed by a single event in $[t_1, t_1 + dt_1)$. The Poisson PDF of the first is simply $e^{-\mu(t_1)}$, where $\mu(t_1) = \int_{-\infty}^{t_1} R(t)dt$ and $R(t)$ is the event rate at time t, i.e., the number of events in the interval $[t, t + dt)$. The PDF of the second is simply $R(t_1)$, leading to the first-event PDF [25]

$$p_1(t_1) = R(t_1)e^{-\mu(t_1)}.$$

The expectation value of the first-event time is then

$$E(t_1) = \frac{\int_{-\infty}^{\infty} t p_1(t)dt}{\int_{-\infty}^{\infty} p_1(t)dt} = \frac{\int_{-\infty}^{\infty} tR(t)e^{-\mu(t)}dt}{\int_{-\infty}^{\infty} R(t)e^{-\mu(t)}dt}. \quad (3)$$

We estimate $E(t_1)$ numerically by using the observed event times t_j in the following manner: we treat the t_j as random variables which are independent (up to the fact that they are sorted), and we approximate the integrals in Eq. (3) in the style of a Monte Carlo integration, as follows:

$$\int_{-\infty}^{\infty} tR(t)e^{-\mu(t)}dt \approx \sum_{j=1}^{N} t_j e^{-\mu(t_j)} \approx \sum_{j=1}^{N} t_j e^{-j}$$

$$\int_{-\infty}^{\infty} R(t)e^{-\mu(t)}dt \approx \sum_{j=1}^{N} e^{-\mu(t_j)} \approx \sum_{j=1}^{N} e^{-j}.$$

In effect, in the first approximation, we treat $R(t)$ in the integrand as a weight function, with larger values indicating a higher density of events. In the second relation, we approximate the cumulative distribution $\mu(t_j)$ with the number of events up to that time, which is simply j. The numerical estimate of $E(t_1)$, which we denote $\langle t_1 \rangle$, is thus

$$E(t_1) \approx \langle t_1 \rangle \equiv \frac{\sum_{j=1}^{N} t_j e^{-j}}{\sum_{j=1}^{N} e^{-j}}, \quad (4)$$

which is essentially a weighted average which emphasizes the early events and exponentially suppresses the later ones. Indeed, it is clear that one needs only the early events to calculate these sums to an appropriate precision. On the other hand, the approximations used above can introduce their own biases; for instance, it is easily shown that $\langle t_1 \rangle > t_1$ by construction, whereas the first-event time could occur before or after the true expectation value $E(t_1)$. It can also be seen that the approximation $\mu(t_j) \approx j$ works best for early times if the rate rises quickly. Conversely, if the rate rises slowly, the approximation can introduce sizable relative deviations from $\mu(t_j)$. It is therefore worth noting that there is good agreement between supernova modeling groups on the rapid rise of the $\bar{\nu}_e$ lightcurve at early times—the channel and phase most relevant to this study [26,27].

If we wish to use the events of a large detector to estimate $\langle t_1 \rangle$ for a smaller detector, we can rescale the larger detector's rate $R(t)$ by a constant factor $\alpha < 1$, such that

$$R'(t) = \alpha R(t).$$

The rescaled estimate corresponding to Eq. (4) then becomes

$$E(t_1^\alpha) \approx \langle t_1^\alpha \rangle \equiv \frac{\sum_{j=1}^{N} t_j e^{-\alpha j}}{\sum_{j=1}^{N} e^{-\alpha j}}. \quad (5)$$

The difference between $\langle t_1 \rangle$ and $\langle t_1^\alpha \rangle$ is the estimated bias of the observed first-event arrival times between two detectors of unequal size.

Compared to Eq. (4), the exponential suppression in Eq. (5) is smaller term by term, and thus can be seen as a weighted average farther into the time series. In fact, it can be proven (see the Appendix) that $\langle t_1^\alpha \rangle > \langle t_1 \rangle$ for $\alpha < 1$. It is also evident that when calculating $\langle t_1^\alpha \rangle$, one should increase the number of early events by a factor of α^{-1} in order to achieve a similar desired level of accuracy.

Now consider two detectors A and B which receive the neutrino signal with a true lag τ_{AB} between them. Experiment A observes N_A events, $\{t_1^A, \ldots, t_{N_A}^A\}$, while experiment B receives $N_B = \alpha N_A$ events, $\{t_1^B, \ldots, t_{N_B}^B\}$. We define the "corrected lag" as

$$Z_{AB} \equiv t_1^A - t_1^B - \langle t_1^A \rangle + \langle t_1^{\alpha A} \rangle, \quad (6)$$

where $\langle t_1^{\alpha A} \rangle$ indicates the rescaled estimate from Eq. (5), based on the event times from detector A. Crucially, $\langle t_1^A \rangle$ and $\langle t_1^{\alpha A} \rangle$ have no lag between them; the only difference in the expectation values is due to the relative yield α. The difference $\langle t_1^A \rangle - \langle t_1^{\alpha A} \rangle$ therefore represents the estimated bias in the first-event difference due only to the relative yields of the two detectors. The expectation value of Z_{AB} is thus, ideally, the true lag itself, i.e., τ_{AB} evaluated with the true supernova direction. We call $Z_{AB} - \tau_{AB}$ the "residual bias," and we use Z_{AB} as our estimate of Δt_{AB} in Eq. (2).

B. Estimated uncertainty

The expected uncertainty on Z_{AB} is determined by noting that t_1^A and t_1^B are independent measurements and hence

$$\sigma_{Z_{AB}}^2 = \sigma_A^2 + \sigma_B^2, \quad (7)$$

where σ_A and σ_B are the uncertainties on t_1^A and t_1^B, respectively. The variance in t_1^A requires estimating the expectation value, following Eq. (3), as follows:

$$E((t_1^A)^2) = \frac{\int_{-\infty}^{\infty} t^2 p_1(t)dt}{\int_{-\infty}^{\infty} p_1(t)dt} \approx \langle (t_1^A)^2 \rangle \equiv \frac{\sum_{j=1}^{N_A} (t_j^A)^2 e^{-j}}{\sum_{j=1}^{N_A} e^{-j}}.$$

The variance in t_1^B, which is invariant with respect to the lag, can be evaluated using the data of detector B, or rescaling the data of detector A, as follows:

$$E((t_1^B - \langle t_1^B \rangle)^2) \approx \langle (t_1^B)^2 \rangle - \langle t_1^B \rangle^2 \approx \langle (t_1^{\alpha A})^2 \rangle - \langle t_1^{\alpha A} \rangle^2.$$

In practice, since the events in both detectors are subject to statistical fluctuations, we evaluate the expectation value with both datasets, and take the larger variance as a conservative estimate of σ_B^2.

If we calculate all time differences with respect to a single "reference" detector, which we designate as A, the covariance matrix of Eq. (2) takes the simple form

$$V = \begin{pmatrix} \sigma_A^2 + \sigma_B^2 & \sigma_A^2 & \sigma_A^2 & \cdots \\ \sigma_A^2 & \sigma_A^2 + \sigma_B^2 & \sigma_A^2 & \\ \sigma_A^2 & \sigma_A^2 & \sigma_A^2 + \sigma_C^2 & \\ \vdots & & & \ddots \end{pmatrix}.$$

Equation (2) then becomes

$$\chi^2(\hat{\mathbf{n}}) = \sum_B \sum_C (\Delta t_{AB} - \tau_{AB}(\hat{\mathbf{n}}))V^{-1}(\Delta t_{AC} - \tau_{AC}(\hat{\mathbf{n}})), \tag{8}$$

where the sums are over all the detectors besides A. This formula is used in Sec. V to evaluate directional confidence intervals with simulated supernovae.

C. Binned data

It is possible, though it will not be implemented for the studies in this article, to derive a similar technique to estimate $E(t_1^\alpha)$ from data which is binned in time, and may include significant background levels. For instance, consider data from experiment A reported as M event counts n_k in time windows $[T_k, T_{k+1})$, with an estimated background b_k in each bin. The time windows do not have to be uniform in length, but they should be long enough such that $n_k - b_k > 0$. Equation (4) then becomes

$$E(t_1) \approx \langle t_1^\alpha \rangle = \frac{\sum_{k=1}^M (n_k - b_k) T_k e^{-\alpha \mu_k}}{\sum_{k=1}^M (n_k - b_k) e^{-\alpha \mu_k}}, \tag{9}$$

where

$$\mu_k = \sum_{r=1}^{k-1} (n_r - b_r)$$

is the background-subtracted sum of event counts before time T_k. Similar expressions can be obtained to provide an estimate of the variance. In this way, neutrino telescopes such as IceCube [28,29] and the Cubic Kilometre Neutrino Telescope (KM3NeT) [30], which have large IBD signal yields but also large backgrounds and cannot identify CCSN neutrino events individually, can be incorporated directly into this supernova multilateration technique. In fact, it is expected that IceCube and KM3NeT will fit their data to determine the start of their neutrino bursts, and will report those times along with their own estimates of the uncertainty, as reported in Refs. [31,32].

TABLE I. True lag times (τ) for the neutrino bursts between pairs of detectors, for the simulated supernova.

Detector 1	Detector 2	True lag (ms)
Super-Kamiokande	JUNO	−1.97
Super-Kamiokande	LVD	−25.15
Super-Kamiokande	SNO+	−14.66
JUNO	LVD	−23.17
JUNO	SNO+	−12.69
LVD	SNO+	10.48

III. SIMULATION

For the purpose of generating event sequences with which to test our method, we utilize the IBD lightcurves of the widely employed `Bollig_2016` [33] models of `SNEWPY` [34,35], assuming a progenitor with $27M_\odot$ and the LS220 equation of state [36]. We also present results using a $11.2M_\odot$ progenitor mass, with the same equation of state, for test purposes.

Unless mentioned otherwise, for all the Monte Carlo trials in this paper, we use the same, but otherwise arbitrary, benchmark supernova time (1 Nov 2021 at 05:22:36.328 GMT) and direction (300° right ascension and −30° declination). The four detectors are modeled using `SNOwGLoBES` [37] assuming a distance of 10 kpc, adiabatic Mikheyev-Smirnov-Wolfenstein oscillations, and normal neutrino mass ordering. The true lag times among the detectors are given in Table I.

IV. RESULTS

A. Before bias correction

We run 100,000 Monte Carlo trials, each including generated IBD events with average yields given in Table II, following Ref. [9]. Figure 1 shows the comparison between the observed first-event time differences, $t_1^A - t_1^B$, before any bias correction, and the true lag τ_{AB}, for all pair combinations of the four detectors. As expected, experiments with similar yields (Super-Kamiokande with JUNO and LVD with SNO+) are centered close to zero, indicating small bias, while pairings of large detectors with small detectors exhibit significant bias. The distributions tend to peak on the negative side, because we have taken detector A

TABLE II. Average IBD event yields assuming a distance of 10 kpc, adiabatic MSW oscillations, and normal neutrino mass ordering, from Ref. [9].

Detector	$27M_\odot$ yield	$11.2M_\odot$ yield
Super-Kamiokande	7800	4000
JUNO	7200	3800
LVD	360	190
SNO+	280	150

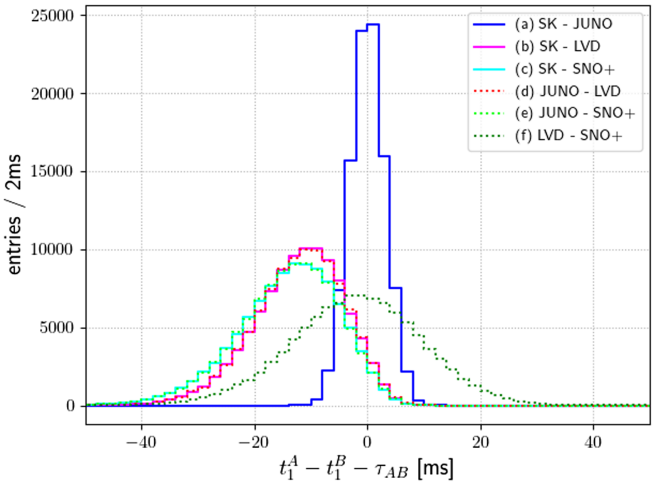

FIG. 1. Before bias correction: distributions of first-event time differences (observed lags) less true lags, $t_1^A - t_1^B - \tau_{AB}$, over 100,000 trials with the $27M_\odot$ IBD lightcurve shape at 10 kpc. Pairwise differences are always computed such that detector A is larger.

always to be the larger one, which on average observes the first event earlier.

We further examine the effect of relative detector yields before any correction by running Monte Carlo trials in which the average Super-Kamiokande yield is held constant, while the average yield is varied at the other detector locations. Figure 2 shows the resulting mean bias as a function of the relative average yield between the smaller and larger detectors, for the two progenitor masses. For the smallest relative yields, comparable to that of pairing

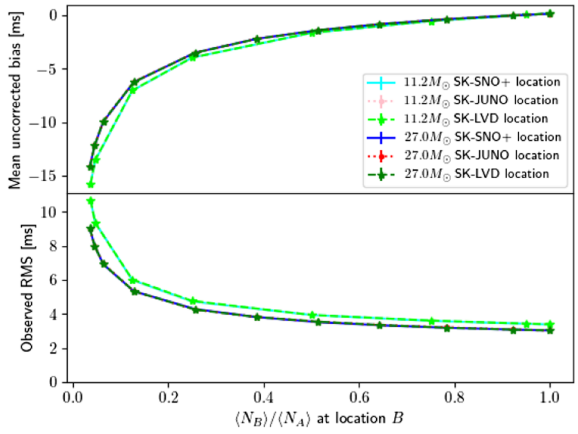

FIG. 2. Top: mean uncorrected bias as a function of relative detector yield for Super-Kamiokande compared with detector locations at JUNO (red/pink), LVD (green/lime green), and SNO+ (blue/cyan). For each value of $\langle N_B \rangle / \langle N_A \rangle$, 100,000 Monte Carlo trials have been run with IBD lightcurves for two progenitor masses ($27M_\odot$ and $11.2M_\odot$). In each case, the average Super-Kamiokande yield is held constant at the value in Table II. Bottom: mean observed rms of the uncorrected distributions. For both figures, the differences between curves for the same progenitor are less than 0.1 ms.

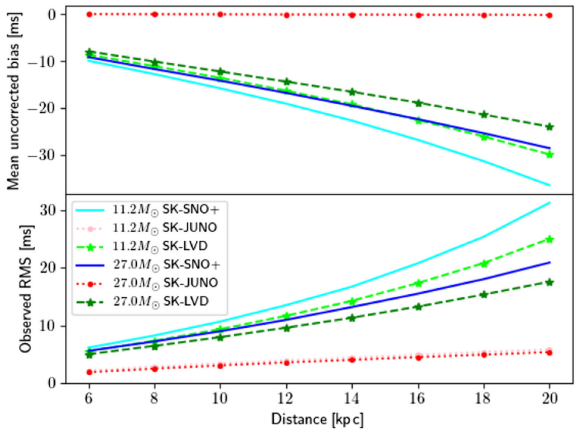

FIG. 3. Top: mean uncorrected bias for Super-Kamiokande compared with other detectors at different distances, using Table II for the yields at 10 kpc. Bottom: mean observed rms of the uncorrected distributions.

Super-Kamiokande with SNO+, the uncorrected bias can exceed 10 ms, while the bias approaches zero as the detector yields become more equal (note that for equal yields, the bias is actually slightly positive, around +0.2 ms, because of the higher energy threshold at Super-Kamiokande). There are small differences between the two progenitors, but for the same progenitor, the bias and its observed rms are largely independent of the detector locations.

In order to examine the effect of varying the overall event yields, we run Monte Carlo trials with nominal yields scaled as if the model supernova has been moved to different distances, from 6 to 20 kpc. The mean uncorrected biases and their mean observed rms are shown as a function of supernova distance in Fig. 3. The biases and observed rms grow with distance, as expected, approaching 30 to 40 ms at 20 kpc.

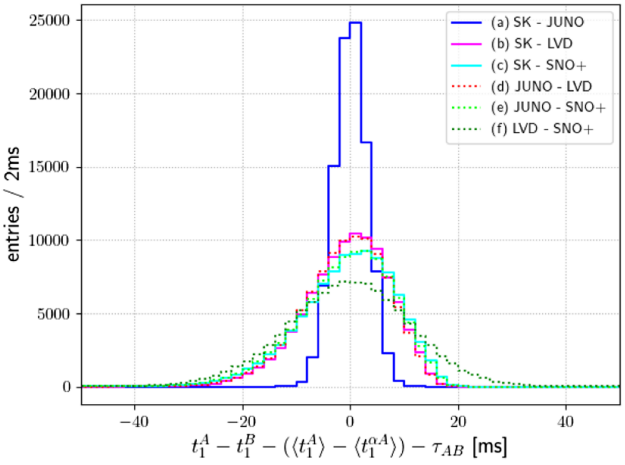

FIG. 4. After bias correction: residual bias (corrected lag less true lag, $Z_{AB} - \tau_{AB}$) distributions over 100,000 trials with the $27M_\odot$ IBD lightcurve shape at 10 kpc.

TABLE III. Observed rms widths of the distributions of $Z_{AB} - \tau_{AB}$, with the $27M_\odot$ IBD lightcurve shape at 10 kpc.

Detector 1	Detector 2	rms (ms) uncorr.	rms (ms) corr.
Super-Kamiokande	JUNO	3.1	3.1
Super-Kamiokande	LVD	8.0	7.8
Super-Kamiokande	SNO+	9.0	8.9
JUNO	LVD	8.0	7.8
JUNO	SNO+	9.0	8.9
LVD	SNO+	11.7	11.5

B. After bias correction

The effect of estimating and correcting for the first-event bias is shown in the $Z_{AB} - \tau_{AB}$ distributions of Fig. 4. As $Z_{AB} - \tau_{AB}$ is the difference between the corrected lag and the true lag, it should ideally be zero. Indeed, the distributions over the Monte Carlo trials are seen to be largely symmetric and centered close to zero, though a negative tail is evident in pairings between larger and smaller detectors. The widths of the distributions of $Z_{AB} - \tau_{AB}$ are listed in Table III, and are all narrower (though just slightly in the case of Super-Kamiokande and JUNO) than the corresponding uncorrected distributions of Fig. 1.

Figure 5 shows the mean residual bias, i.e., the mean of the $Z_{AB} - \tau_{AB}$ distribution, as a function of the relative average yields. The behavior of the mean residual bias is largely uniform across different detector locations, and therefore across true lag values. Even with the smallest detector, SNO+, expecting 280 events at 10 kpc from the $27M_\odot$ model, the residual bias is less than 1 ms, compared with nearly 15 ms before correction, an improvement better than a factor of 10. As the yields become more symmetric, this improvement is less noticeable (as before, the mean residual bias actually approaches +0.2 ms due to the aforementioned higher energy threshold for Super-Kamiokande). The mean

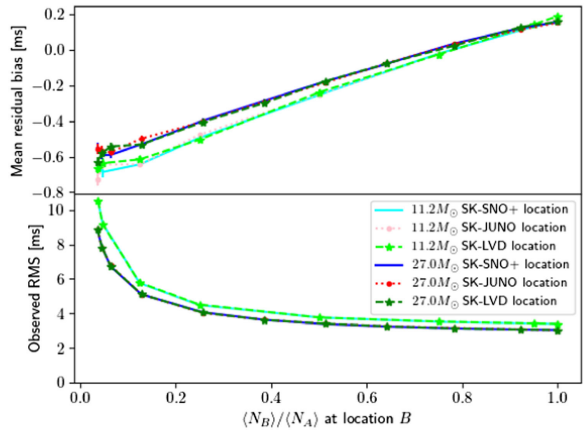

FIG. 5. Top: mean residual bias as a function of relative detector yield, after correcting for the first-event bias, for Super-Kamiokande compared with detector locations at JUNO, LVD, and SNO+. Bottom: mean observed rms after first-event bias correction.

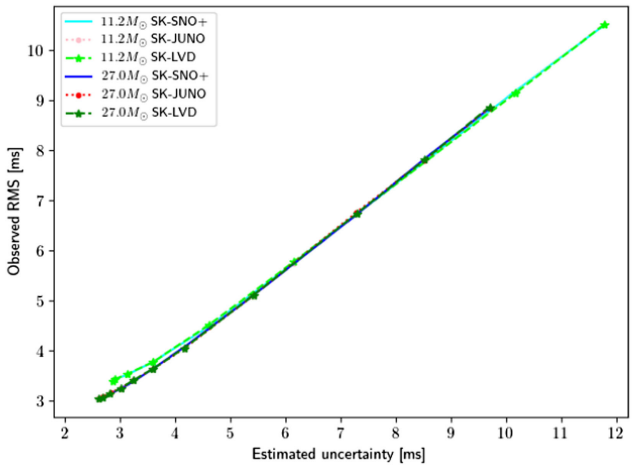

FIG. 6. Mean observed rms as a function of the mean estimated uncertainty from Eq. (7) for the IBD lightcurve shape.

observed rms, which reflects the measurement uncertainty for any single trial (i.e., supernova event), decreases from around 10 ms to a minimum variability of around 3 ms with increasing relative yield. For all relative yields, the residual bias is much smaller than the observed rms.

Figure 6 compares the observed rms with the estimated uncertainty calculated using Eq. (7). The relationship between the observed and expected values is mostly linear, though saturating in the $27.0M_\odot$ model at 2.6 ms for the mean of the expected uncertainties, and about 3.1 ms for the corresponding observed rms; these values reflect the inherent statistical uncertainty when comparing two detectors with the same average yields of 7800 events. The fact that the calculated uncertainty differs from the observed variability is not surprising given the approximations used. In simplified numerical cases, replacing $\mu(t_j)$ with j by itself can be shown to account for differences of a similar size. In order to draw reasonable confidence intervals from the data of a single supernova, in the following we will use the estimated uncertainty and inflate it by a factor of 1.2

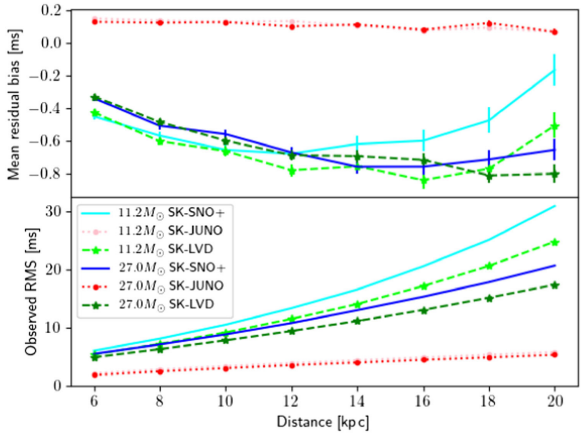

FIG. 7. Mean residual bias and mean observed rms using the IBD shape, but at different distances.

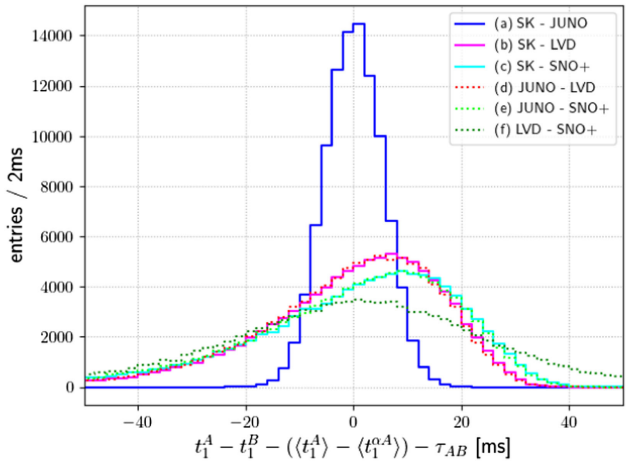

FIG. 8. Residual bias distributions over 100,000 trials with the $27M_\odot$ IBD lightcurve shape, but at 20 kpc distance.

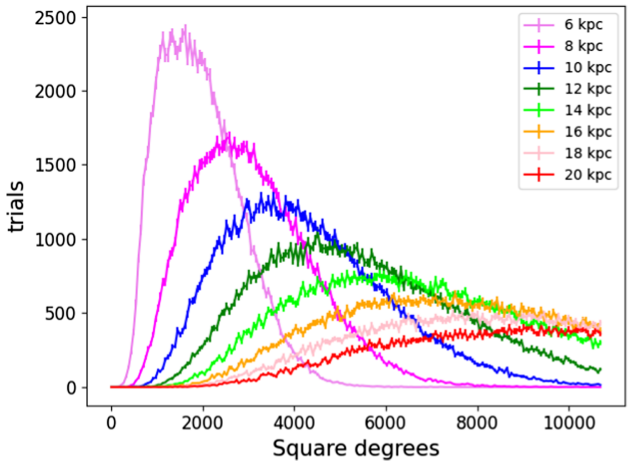

FIG. 10. Coverage areas, in square degrees, of the 68% confidence interval, for the $27M_\odot$ model at distances from 6 to 20 kpc.

(the ratio between the expected and observed rms values), even though this straightforward inflation generally overestimates the measurement uncertainty at lower yields (see Sec. V). The corresponding values in the $11.2M_\odot$ model, with a top average yield of 4000 events, are 3.4 ms observed and 2.9 ms expected, also giving a ratio of 1.2.

The mean residual biases and mean observed rms are shown as a function of supernova distance in Fig. 7. As with the uncorrected means in Fig. 3, the biases and observed rms grow with distance. The pattern changes, however, for smaller detectors and distances above about 12 kpc. The reason is illustrated in Fig. 8: for pairings between a large and a small detector, the peak of the $Z_{AB} - \tau_{AB}$ distribution has shifted toward positive values, while a sizable negative tail has grown, in some cases pulling the mean back to small values. The shift is likely related to the asymmetry in the approximation noted after Eq. (4): while for a pair of detectors with similar yields, such as Super-Kamiokande and JUNO, the asymmetries largely cancel out in the difference in Z_{AB}, lower yields exacerbate the asymmetry, and their effects do not cancel when detectors of very different yields are paired. Indeed, the peaks of those pairings all appear on the positive side, indicating an overcorrection of the bias.

V. POINTING

We combine the time differences into a direction by calculating the χ^2 of Eq. (8) between the observed time differences (with bias correction) and the predicted time differences for different test directions. We use the centers of the equal-area HEALPix [38,39] pixels, in the equatorial International Celestial Reference System (ICRS, or "celestial") frame, as the test directions $\hat{\mathbf{n}}$, and assign the χ^2 for that direction to each pixel. Super-Kamiokande is designated the reference detector A, and the uncertainty estimates are inflated by the factor 1.2, as suggested in Sec. IV. We then find the minimum χ^2 value from among all the pixels and subtract that value from all of them. Each pixel is assigned the probability associated with the (subtracted) χ^2 value, assuming two degrees of freedom. The resulting probability skymaps, with HEALPix $N_{\text{side}} = 32$, are shown in Fig. 9 for three CCSN explosions simulated with the $27M_\odot$ model at a distance of 10 kpc. As shown in Fig. 10, the areas covered by the 68% confidence interval can range from approximately 1000 to 10,000 square degrees for this supernova model and distance, with the distributions expanding and contracting with distance as expected. An overall probability skymap for 10 kpc,

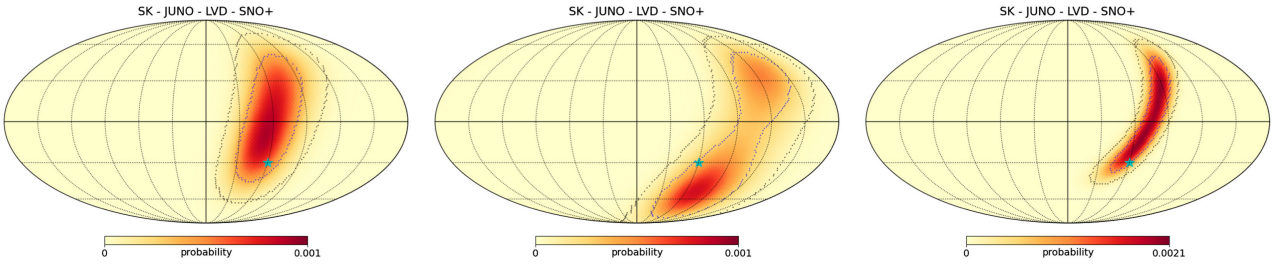

FIG. 9. Sample probability skymaps for three different Monte Carlo trials combining the four detectors. The 68% confidence intervals are marked out by purple dots, with areas 3770, 5440, and 1520 square degrees, from left to right. The 95% confidence intervals, marked out by black dots, cover 8800, 11,800, and 3490 square degrees. The true location for all the trials is indicated by the light blue star.

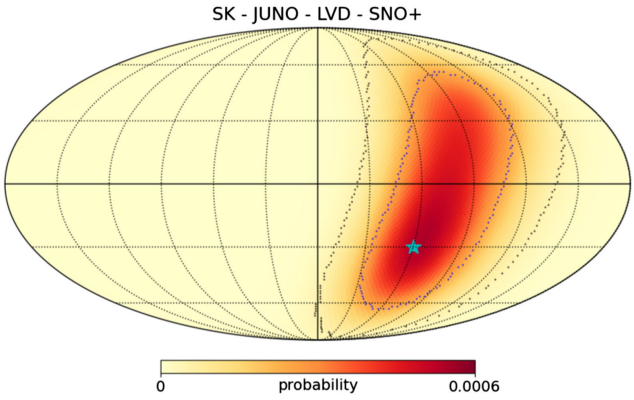

FIG. 11. Probability skymap averaged over 100,000 Monte Carlo trials, with 68% (purple) and 95% (black) confidence intervals after first-event bias correction. The true location is indicated by the light blue star.

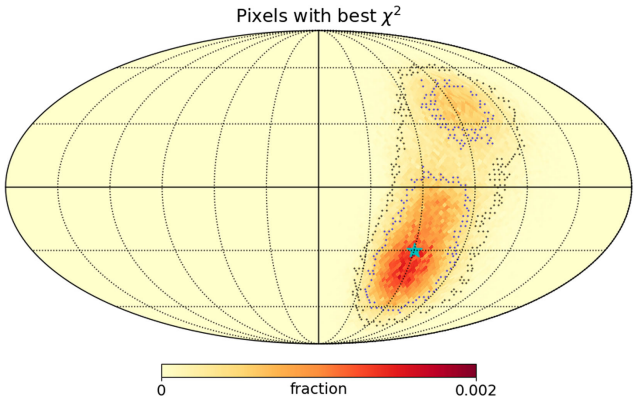

FIG. 13. Skymap built with pixels of maximum probability over 100,000 trials. Regions including 68% and 95% of the best pixels are marked out by the purple and black dots, respectively. The true supernova location is indicated with the light blue star.

averaged over 100,000 trials, is shown in Fig. 11. This skymap can be compared with Fig. 12, which has been calculated in the same way, but without the first-event correction; in spite of the true supernova position perching on the edge of the 68% confidence region, it is likely that the best observers will be looking in the wrong direction.

One way to test the coverage is to count the number of times, among the 100,000 trials, any given pixel is deemed most likely, i.e., has the minimum χ^2. The resulting skymap, shown in Fig. 13, resembles the probability maps of Figs. 9 and 11, though with somewhat smaller 68% and 95% regions, reflecting overcoverage by the estimated uncertainties.

A more quantitative test of the coverage can be performed by calculating the confidence interval to which the true direction has been assigned. For this purpose, we plot the value of the χ^2 cumulative probability distribution function for the χ^2 for the pixel containing the true direction. The result is shown in Fig. 14, both before and after bias correction. Ideally, the histogram would be flat, with (for instance) 68% of the histogram below the value 0.68, i.e., with the true position lying within the 68% region 68% of the time. Instead, aside from a small spike near 1, the histogram before bias correction is decidedly not flat, with just 38% (86%) of the trials having the true position assigned a value of 0.68 (0.95), while the histogram after bias correction is more flat, with the true position lying within the purported 68% (95%) confidence intervals 73% (92%) of the time. The spike near 1, present in both histograms, is attributed to the effects of non-Gaussian tails in the corresponding time difference distributions, even after bias correction (Figs. 1 and 4).

It is instructive to look at how the method works for different supernova directions. We place supernovae at the centers of each of the 3072 HEALPix pixels with $N_{\text{side}} = 16$, and generate 10,000 Monte Carlo trials at each location. The mean residual biases and widths are consistent across the sky. The resulting confidence intervals, however, do vary in size with different supernova directions due to their orientations with respect to the detectors.

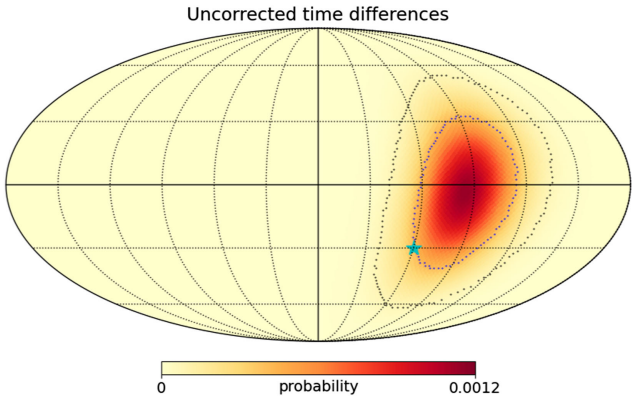

FIG. 12. Probability skymap averaged over 100,000 Monte Carlo trials without first-event bias correction. The true location is indicated by the light blue star.

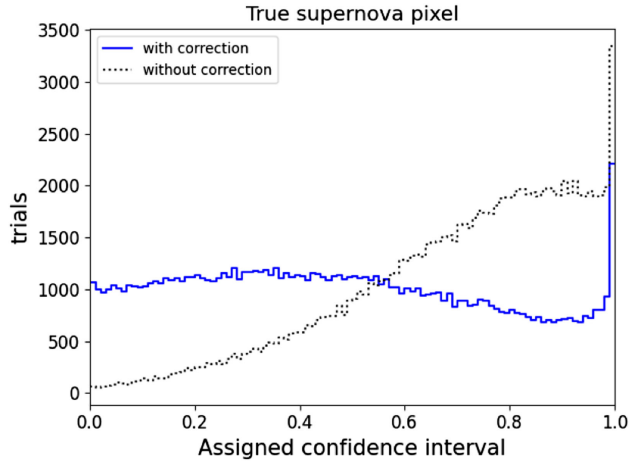

FIG. 14. Confidence interval assigned to the pixel of the true supernova direction, with bias correction (blue solid) and without (black dotted).

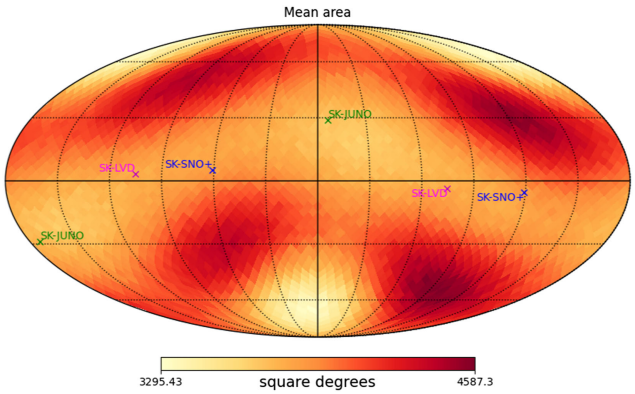

FIG. 15. Average coverage areas in square degrees of the 68% confidence interval, for directions defined by the centers of $N_{\text{side}} = 16$ HEALPix pixels.

The mean areas of the 68% confidence intervals are shown in Fig. 15, along with the directions defined by the detector pairs at the benchmark supernova time. The area varies from about 3300 to 4600 square degrees, with the larger areas off the detector-pair axes. The banded structure of the skymap is evidently due to the fact that all the detectors operate in a narrow band of latitude, from about 22° to 46°, all in the northern hemisphere. The structure highlights the value of greater geographical spread among the detectors, including, of course, detectors such as IceCube.

Figure 16 shows the 68% confidence interval coverage in each direction, computed in terms of the fraction of the 10,000 trials in which the true direction is included in the 68% confidence interval. As shown in Fig. 17, the fraction varies from 0.67 to 0.85, with the most frequent fraction around 69%. The behavior is consistent with the expectation that inflating the uncertainty estimate by the factor 1.2 leads to largely appropriate, but sometimes conservative, confidence intervals. The nominal supernova direction used in Sec. IV and this section happened to point to a region of the sky with slightly conservative intervals, with (as noted above) the true pixel lying in the 68% interval 73% of the time.

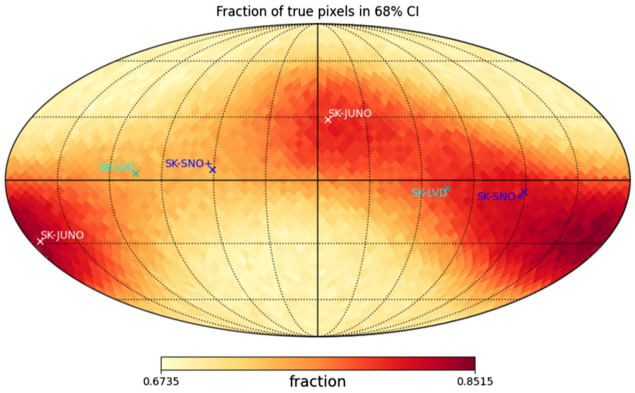

FIG. 16. Fractions of the 10,000 trials at each direction which are included in the 68% confidence interval.

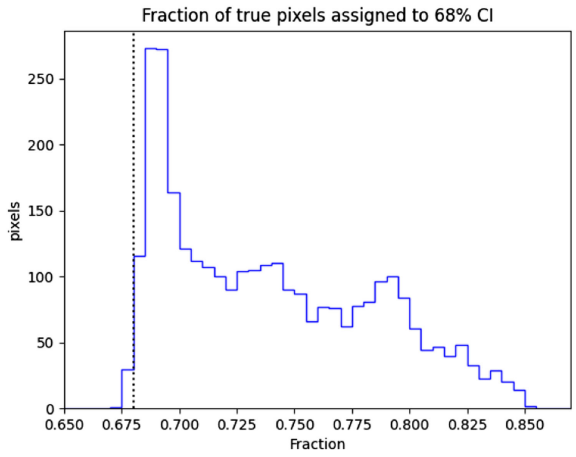

FIG. 17. Histogram of fractions in Fig. 16 over the 3072 pixels of the $N_{\text{side}} = 16$ HEALPix skymap.

VI. DISCUSSION

In this article, we have further developed the first-event method by deriving a data-driven approach for reducing the time difference bias due to two detectors' differing event yields. The method requires only the times of the first events at most detectors, along with a longer time series from one larger detector to act as a reference lightcurve. The time delay between the first IBD events in different detectors, along with its estimated uncertainty, have then been used for the purpose of localizing the supernova via multilateration. The method has been tested in Monte Carlo trials with the `Bollig_2016` models in `SNEWPY`. At a distance of 10 kpc, the residual bias is reduced from over 10 ms to less than 1 ms when two detectors differ in size by more than an order of magnitude, a pattern which holds even when the distance is increased to 20 kpc. We have also demonstrated how the uncertainty can be estimated directly from the data, and that the resulting probability skymaps resemble those generated from Monte Carlo trials. Moreover, the estimated uncertainties result in confidence intervals which are reasonable, tending to the somewhat conservative, over all sky directions. The 68% confidence interval covers several thousand square degrees. While this area is much larger than the approximately 30 to 150 square degrees ultimately expected to be possible with elastic scatters, the present method is suitable for a quick, real-time estimate in SNEWS2.0.

The main assumptions in this method are (i) that background can be neglected in the contributing detectors over the supernova burst timescale, (ii) that the shape of the time profile of the event rate is similar for all of them, and (iii) that the early part of the event rate shape is characterized by a single, rapid rise. These assumptions are reasonable for coincidence-tagged IBD events in at least several large underground water Cherenkov and liquid scintillator detectors. Where the background level is high, as in neutrino telescopes like IceCube and KM3NeT,

the assumption of a single rapid rise may still lead to a well-defined starting time similar to the expected first-event time $\langle t_1 \rangle$, such that after background subtraction a useful time difference can be integrated into first-event multilateration. A formula for using binned data with large backgrounds has also been derived [Eq. (9)]. It should be noted that the burst starting time used here is *not* the same as the bounce time, since calculating the latter requires more sophisticated model-based assumptions.

It is expected that SNEWS2.0 will employ multiple algorithms to multilaterate the supernova direction under different assumptions and levels of model dependence. At least some methods should minimize model dependence, as the present method does. Moreover, the first-event method can also be used as an initial direction which can be refined by slower but more precise methods that utilize features of the entire lightcurve. For instance, algorithms using more information about the lightcurve can take advantage of distinctive features that may occur later in the supernova, such as the rapid flux decrease due to the formation of a black hole $O(1)$ second after the initial bounce [12,40,41]. In this way, the global multimessenger community can increase the chance to take full advantage of one of the most brilliant events in the Galaxy.

Plots were generated with Matplotlib [42], and some results derived using the HEALPY [43] and HEALPix packages.

ACKNOWLEDGMENTS

F. A. and J. T. acknowledge support from the Science and Technology Facilities Council (STFC), United Kingdom. M. C. M. acknowledges the support of the Belgian Fund for Scientific Research, the FRS-FNRS (Fond pour le Recherche Scientifique). K. S., A. H., and S. B. acknowledge NSF support from Grant No. PHY-2209534, J. K. from Grant No. PHY-2209449, and D. M. from Grants No. PHY-2209451 and No. AST-2206532. E. O. is supported by the Swedish Research Council (Project No. 2020-00452).

DATA AVAILABILITY

The data that support the findings of this article are openly available [34,35,44].

APPENDIX: FIRST-EVENT TIMES FOR SMALLER EXPERIMENTS

We can see that $\langle t_1^\alpha \rangle > \langle t_1 \rangle$ for all $\alpha < 1$ by differentiating with respect to α as α decreases. We start from the difference formula

$$-\frac{d\langle t_1^\alpha \rangle}{d\alpha} = \lim_{\epsilon \to 0} \frac{\langle t_1^{\alpha-\epsilon} \rangle - \langle t_1^\alpha \rangle}{\epsilon}. \tag{A1}$$

The numerator is

$$\frac{\sum_{j=1}^N t_j e^{-(\alpha-\epsilon)j}}{\sum_{j=1}^N e^{-(\alpha-\epsilon)j}} - \frac{\sum_{j=1}^N t_j e^{-\alpha j}}{\sum_{j=1}^N e^{-\alpha j}},$$

which to first order in ϵ (higher orders vanishing in the limit) is

$$\frac{(\sum_j t_j j e^{-\alpha j})(\sum_k e^{-\alpha k}) - (\sum_j t_j e^{-\alpha j})(\sum_k k e^{-\alpha k})}{(\sum_j e^{-\alpha j})^2}.$$

The denominator is always positive, so we concentrate on the numerator, which becomes

$$\sum_{j=1}^N \sum_{k=1}^N t_j (j-k) e^{-\alpha(j+k)} = \sum_{j=1}^N \sum_{k=1}^N t_j w_{jk}, \tag{A2}$$

where $w_{jk} \equiv (j-k)e^{-\alpha(j+k)}$. It is easy to see that w_{jk} is antisymmetric in its indices and $w_{jk} > 0$ whenever $j > k$. We split the sum into lower and upper triangular regions in (j,k), as follows:

$$\sum_{j=1}^N \sum_{k=1}^{j-1} t_j w_{jk} + \sum_{j=1}^N \sum_{k=j+1}^N t_j w_{jk}.$$

The terms in the second double sum can be reordered before swapping the dummy indices, as follows:

$$\begin{aligned} \sum_{j=1}^N \sum_{k=j+1}^N t_j w_{jk} &= \sum_{k=1}^N \sum_{j=1}^{k-1} t_j w_{jk} \\ &= \sum_{j=1}^N \sum_{k=1}^{j-1} t_k w_{kj} \\ &= -\sum_{j=1}^N \sum_{k=1}^{j-1} t_k w_{jk}. \end{aligned}$$

The expression in Eq. (A2) is now

$$\sum_{j=1}^N \sum_{k=1}^N t_j w_{jk} = \sum_{j=1}^N \sum_{k=1}^{j-1} (t_j - t_k) w_{jk}.$$

We know that since $j > k$ for all terms in the sum, $w_{jk} > 0$. Moreover, $t_j - t_k > 0$ because the event times are ordered in increasing time. The expression in Eq. (A1) thus is positive, and $\langle t_1^\alpha \rangle$ increases monotonically, as α decreases. It is thus shown that when using a single dataset to estimate the expectation values of the first-event time at smaller experiments, that expectation value trends later as the experiment gets smaller, as one would expect.

[1] See, for instance, Refs. [2–4], and recent articles such as Refs. [5–7].

[2] Y. Koshio, G. D. O. Gann, E. O'Sullivan, and I. Tamborra, Snowmass 2021 topical group report: Neutrinos from natural sources, arXiv:2209.04298.

[3] S. Furusawa and H. Nagakura, Nuclei in core-collapse supernovae engine, Prog. Part. Nucl. Phys. **129**, 104018 (2023).

[4] A. Arcones *et al.*, White paper on nuclear astrophysics and low energy nuclear physics Part 1: Nuclear astrophysics, Prog. Part. Nucl. Phys. **94**, 1 (2017).

[5] L. Visinelli, T. T. Yanagida, and M. Zantedeschi, Do neutrinos bend? Consequences of an ultralight gauge field as dark matter, Phys. Dark Universe **46**, 101659 (2024).

[6] A. Lella, E. Ravensburg, P. Carenza, and M. C. D. Marsh, Supernova limits on 'QCD axion-like particles', Phys. Rev. D **110**, 043019 (2024).

[7] C. Li, Z. Liu, W. Lu, and Z. Ye, Low-energy supernova constraints on millicharged particles, J. High Energy Phys. 07 (2025) 116.

[8] K. Rozwadowska, F. Vissani, and E. Cappellaro, On the rate of core collapse supernovae in the Milky Way, New Astron. **83**, 101498 (2021).

[9] S. Al Kharusi *et al.* (SNEWS Collaboration), SNEWS 2.0: A next-generation supernova early warning system for multi-messenger astronomy, New J. Phys. **23**, 031201 (2021).

[10] J. F. Beacom and P. Vogel, Can a supernova be located by its neutrinos?, Phys. Rev. D **60**, 033007 (1999).

[11] T. Mühlbeier, H. Nunokawa, and R. Zukanovich Funchal, Revisiting the triangulation method for pointing to supernova and failed supernova with neutrinos, Phys. Rev. D **88**, 085010 (2013).

[12] V. Brdar, M. Lindner, and X.-J. Xu, Neutrino astronomy with supernova neutrinos, J. Cosmol. Astropart. Phys. 04 (2018) 025.

[13] N. B. Linzer and K. Scholberg, Triangulation pointing to core-collapse supernovae with next-generation neutrino detectors, Phys. Rev. D **100**, 103005 (2019).

[14] A. Coleiro, M. Colomer Molla, D. Dornic, M. Lincetto, and V. Kulikovskiy, Combining neutrino experimental light-curves for pointing to the next galactic core-collapse supernova, Eur. Phys. J. C **80**, 856 (2020).

[15] Y. Kashiwagi *et al.* (Super-Kamiokande Collaboration), Performance of SK-Gd's upgraded real-time supernova monitoring system, Astrophys. J. **970**, 93 (2024).

[16] A. Abed Abud *et al.* (DUNE Collaboration), Supernova pointing capabilities of DUNE, Phys. Rev. D **111**, 092006 (2025).

[17] Y. Fukuda *et al.* (Super-Kamiokande Collaboration), The Super-Kamiokande detector, Nucl. Instrum. Methods Phys. Res., Sect. A **501**, 418 (2003).

[18] A. Abusleme *et al.* (JUNO Collaboration), JUNO physics and detector, Prog. Part. Nucl. Phys. **123**, 103927 (2022).

[19] M. Aglietta *et al.*, The most powerful scintillator supernovae detector: LVD, Nuovo Cimento Soc. Ital. Fis. **105A**, 1793 (1992).

[20] V. Albanese *et al.* (SNO+ Collaboration), The SNO + experiment, J. Instrum. **16**, P08059 (2021).

[21] A. Odrzywolek, M. Misiaszek, and M. Kutschera, Detection possibility of the pair—annihilation neutrinos from the neutrino—cooled pre-supernova star, Astropart. Phys. **21**, 303 (2004).

[22] A. Odrzywolek, M. Misiaszek, and M. Kutschera, Neutrinos from pre-supernova star, Acta Phys. Pol. B **35**, 1981 (2004).

[23] K. M. Patton, C. Lunardini, and R. J. Farmer, Presupernova neutrinos: Realistic emissivities from stellar evolution, Astrophys. J. **840**, 2 (2017).

[24] K. M. Patton, C. Lunardini, R. J. Farmer, and F. X. Timmes, Neutrinos from beta processes in a presupernova: Probing the isotopic evolution of a massive star, Astrophys. J. **851**, 6 (2017).

[25] V. Brdar and X.-J. Xu, Timing and multi-channel: Novel method for determining the neutrino mass ordering from supernovae, J. Cosmol. Astropart. Phys. 08 (2022) 067.

[26] E. O'Connor *et al.*, Global comparison of core-collapse supernova simulations in spherical symmetry, J. Phys. G **45**, 104001 (2018).

[27] R. M. Cabezón, K.-C. Pan, M. Liebendörfer, T. Kuroda, K. Ebinger, O. Heinimann, F.-K. Thielemann, and A. Perego, Core-collapse supernovae in the hall of mirrors. A three-dimensional code-comparison project, Astron. Astrophys. **619**, A118 (2018).

[28] M. G. Aartsen *et al.* (IceCube Collaboration), The IceCube neutrino observatory: Instrumentation and online systems, J. Instrum. **12**, P03012 (2017).

[29] R. Abbasi *et al.* (IceCube Collaboration), An end-to-end test of the sensitivity of IceCube to the neutrino burst from a core-collapse supernova, Proc. Sci., ICRC2021 (**2021**) 1085 [arXiv:2107.08098].

[30] S. Adrian-Martinez *et al.* (KM3Net Collaboration), Letter of intent for KM3NeT 2.0, J. Phys. G **43**, 084001 (2016).

[31] R. Cross, A. Fritz, and S. Griswold (IceCube Collaboration), Eleven year search for supernovae with the IceCube neutrino observatory, Proc. Sci., ICRC2019 (**2020**) 889 [arXiv:1908.07249].

[32] S. Aiello *et al.* (KM3NeT Collaboration), The KM3NeT potential for the next core-collapse supernova observation with neutrinos, Eur. Phys. J. C **81**, 445 (2021).

[33] A. Mirizzi, I. Tamborra, H.-T. Janka, N. Saviano, K. Scholberg, R. Bollig, L. Hudepohl, and S. Chakraborty, Supernova neutrinos: Production, oscillations and detection, Riv. Nuovo Cimento **39**, 1 (2016).

[34] A. L. Baxter *et al.* (The SNEWS Collaboration), SNEWPY: A data pipeline from supernova simulations to neutrino signals, Astrophys. J. **925**, 107 (2022).

[35] A. L. Baxter *et al.*, SNEWPY: A data pipeline from supernova simulations to neutrino signals, J. Open Source Software **6**, 3772 (2021).

[36] S. E. Woosley and A. Heger, Nucleosynthesis and remnants in massive stars of solar metallicity, Phys. Rep. **442**, 269 (2007).

[37] A. Beck *et al.*, https://github.com/SNOwGLoBES/snowglobes (2016).

[38] K. M. Górski, E. Hivon, A. J. Banday, B. D. Wandelt, F. K. Hansen, M. Reinecke, and M. Bartelmann, HEALPix: A framework for high-resolution discretization and fast analysis of data distributed on the sphere, Astrophys. J. **622**, 759 (2005).

[39] http://healpix.sf.net/
[40] J.-S. Wang, J. Tseng, S. Gullin, and E. P. O'Connor, Nonradial neutrino emission upon black hole formation in core collapse supernovae, Phys. Rev. D **104**, 104030 (2021).
[41] S. Gullin, E. P. O'Connor, J.-S. Wang, and J. Tseng, Neutrino echos following black hole formation in core-collapse supernovae, Astrophys. J. **926**, 212 (2022).
[42] J. D. Hunter, Matplotlib: A 2d graphics environment, Comput. Sci. Eng. **9**, 90 (2007).
[43] A. Zonca, L. Singer, D. Lenz, M. Reinecke, C. Rosset, E. Hivon, and K. Gorski, HEALPY: Equal area pixelization and spherical harmonics transforms for data on the sphere in Python, J. Open Source Softwaare **4**, 1298 (2019).
[44] A. L. Baxter *et al.*, SNEWPY: Supernova neutrino early warning models for Python, 10.21105/joss.03772 (2021).